A Nanoparticle Approach To Control the Phase Separation in Polyfluorene Photovoltaic Devices

Thomas Kietzke,[†] Dieter Neher,*[,†] Michael Kumke,[‡] Rivelino Montenegro,[§] Katharina Landfester,[⊥] and Ullrich Scherf[#]

Institute of Physics, University of Potsdam, Am Neuen Palais 10, 14469 Potsdam, Germany; Institute of Chemistry, University of Potsdam, Karl-Liebknecht-Str. 24−25, 14476 Golm, Germany; Department of Chemical Engineering and Applied Chemistry, University of Toronto, 200, College St., M5A 3X1 Toronto, Canada; Macromolecular Chemistry, University of Ulm, Albert-Einstein-Allee 11, 89069 Ulm, Germany; and Department of Chemistry, University of Wuppertal, Gaussstrasse 20, 42097 Wuppertal, Germany

Received February 25, 2004; Revised Manuscript Received April 29, 2004

ABSTRACT: Polymer solar cell devices with nanostructured blend layers have been fabricated using single- and dual-component polymer nanospheres. Starting from an electron-donating and an electron-accepting polyfluorene derivative, PFB and F8BT, dissolved in suitable organic solvents, dispersions of solid particles with mean diameters of ca. 50 nm, containing either the pure polymer components or a mixture of PFB and F8BT in each particle, were prepared with the miniemulsion process. Photovoltaic devices based on these particles have been studied with respect to the correlation between external quantum efficiency and layer composition. It is shown that the properties of devices containing a blend of single-component PFB and F8BT particles differ significantly from those of solar cells based on blend particles, even for the same layer composition. Various factors determining the quantum efficiency in both kinds of devices are identified and discussed, taking into account the spectroscopic properties of the particles. An external quantum efficiency of ca. 4% is measured for a device made from polymer blend nanoparticles containing PFB:F8BT at a weight ratio of 1:2 in each individual nanosphere. This is among the highest values reported so far for photovoltaic cells using this material combination.

Introduction

Photovoltaic devices based on semiconducting polymers have been shown to exhibit high external quantum efficiencies. Because of the high absorption coefficient, e.g., compared to silicon, a layer thickness of less than 1 μm is necessary to absorb all light, thus allowing for ultrathin flexible devices. The best efficiencies were reported for blends or bilayer systems consisting of a hole-accepting polymer and an electron acceptor, such as electron-accepting polymers or fullerene derivatives, relying on the field-induced charge separation between the two components.[1−3] One main problem when using semiconducting polymers is, however, that excitons travel at most few tens of nanometers before they decay radiatively or nonradiatively back to the ground state. Thus, efficient charge generation requires that most excitons are generated within a short distance of the interface between the electron-donating and -accepting phase.

Since the entropy of mixing of polymers is relatively low, mixtures of polymers deposited from organic solvents tend to phase separate during the evaporation of the solvent. The length scale on which this phase separation occurs depends on a variety of parameters such as the individual solubility of the polymers in the solvent, the interaction with the substrate, the layer thickness, the evaporation speed of the solvent, and the annealing temperature.[4−10] Since a direct and universal method to control the phase separation in layers prepared from polymers dissolved in organic solvent did not exist, most attempts to optimize photovoltaic devices with polymer blends rely on trial and error. Several approaches were undertaken to form well-defined and controlled multicomponent polymer structures on the nanometer scale including the use of block copolymers.[11−13] However, this approach is rather limited because both components have to be connected by a covalent bond. Therefore, these copolymers have seldom been used for organic solar cell devices.

Recently, a combination of two polyfluorene-based polymers has been studied in detail with respect to the correlation between layer composition, morphology, and photovoltaic properties.[10,14−22] PFB [poly(9,9-dioctylfluorene-2,7-diyl-*co*-bis-*N*,*N*'-(4-butylphenyl)-bis-*N*,*N*'-phenyl-1,4-phenylenediamine)][23] is known to be a high mobility hole-transporting polymer, whereas F8BT [poly(9,9-dioctylfluorene-2,7-diyl-*co*-benzothiadiazole)][24] (Figure 1a) shows a relatively high electron mobility. The ionization potentials were measured for F8BT to be around 5.9 eV [24,25] and 5.1 eV for PFB.[23] Assuming an exciton binding energy of 0.3 eV, the electron affinity can be calculated by subtracting this value and the optical band gap (2.4 eV for F8BT and 2.9 eV for PFB) from the ionization potentials. Following these arguments, F8BT should have the lowest unoccupied molecular orbital (LUMO) at 3.2 eV and the highest occupied molecular orbital (HOMO) at 5.9 eV, whereas PFB has a LUMO energy of 1.9 eV and a HOMO energy of 5.1 eV. Apparently, there exists a relatively large offset of 1.3 eV for the LUMO levels and of 0.8 eV for the HOMO levels, which guarantees very efficient electron dissociation at the interface.

[†] Institute of Physics, University of Potsdam.
[‡] Institute of Chemistry, University of Potsdam.
[§] University of Toronto.
[⊥] University of Ulm.
[#] University of Wuppertal.
* Corresponding author. E-mail neher@rz.uni-potsdam.de.

10.1021/ma049625y CCC: $27.50
Published on Web 06/03/2004

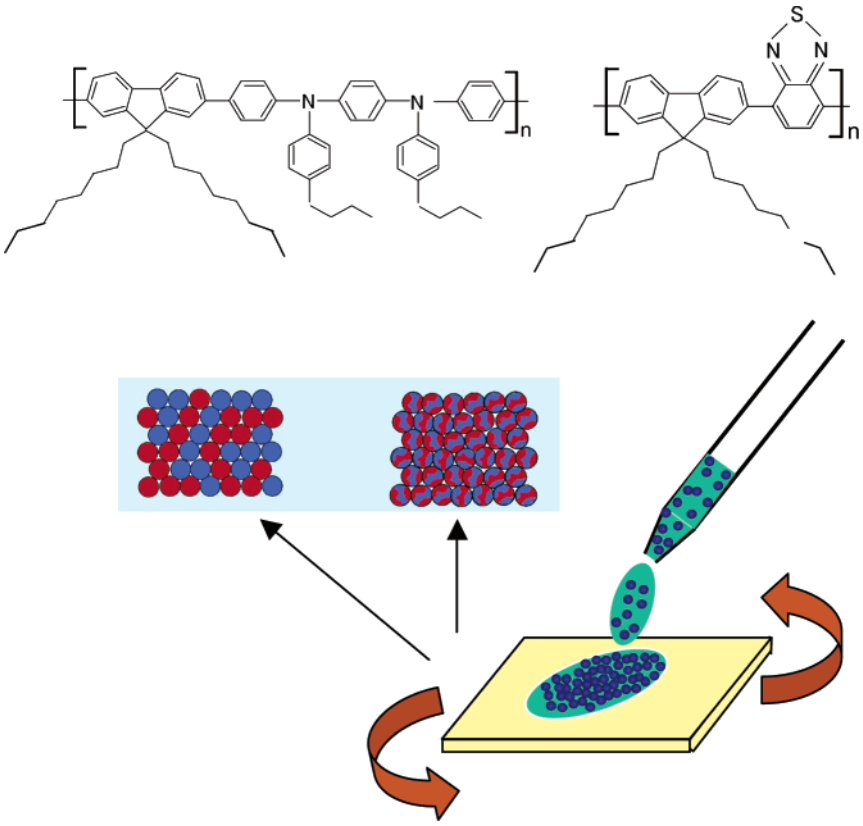

Figure 1. (a, top) Chemical structures of PFB and F8BT. (b, bottom) Spin-coating either a mixture of different particles or particles containing a blend of polymers.

Investigations concerning its blend morphology in relation to the solar cell properties revealed that the length scale on which phase separation occurs does strongly depend on the solvent used, the interaction with the substrate, and deposition conditions.[10,14,15,18−21]

For example, spin-coating a 1:1 PFB:F8BT solution from *p*-xylene leads to a phase separation in the micrometer range whereas the length scale of the phase separation for films prepared from chloroform solution is less than 100 nm. This can be explained by the fact that the more rapid evaporation of the low boiling point solvent chloroform compared to *p*-xylene prevents large-scale reorganization and diffusion of the polymer chains and thus leads to a finer scale of the phase separation.

To compare the spectral response of different solar cells, the external quantum efficiency or incident-photon-to-converted-electron efficiency (IPCE) is widely used. It is defined by

$$\mathrm{IPCE} = \frac{\text{no. of electrons}}{\text{no. of photons}} = \frac{hcI_{\mathrm{SC}}}{e\lambda P_{\mathrm{light}}}$$

where λ is the incident wavelength, I_{SC} the short-circuit current, e the elementary charge, h the Planck constant, c the speed of light, and P_{light} the incident light power. For the 1:1 PFB:F8BT blends the IPCE was ca. 2 times larger for layers spin-coated from chloroform (IPCE = 2−4.5%) solution compared to *p*-xylene solutions (IPCE = 0.5−1%).[15,20] Note that devices incorporating only one kind of polymer exhibited a much lower efficiency of 0.3% (F8BT) or even below 0.1% (PFB).[20] The same group also demonstrated bilayer devices fabricated by a lamination technique, which achieved IPCE efficiencies of up to 1.2%. In up-following studies, the optimization of photovoltaic devices had been done by varying the ratios of PFB and F8BT in layers prepared from *p*-xylene solution. It was found that the phase separation and the external quantum efficiencies were strongly depended on the layer composition. Highest efficiencies have been reported for devices containing 5 times more of the electron-transporting F8BT than PFB.[20] On the other hand, the highest degree of photoluminescence (PL) quenching (being indicative of efficient exciton dissociation at the polymer−polymer interface) was reported for layers comprising of PFB and F8BT in a ratio of 5:1. For theses layers AFM and Raman microscopy investigations revealed a substructure in the nanometer range in addition to a mesoscale phase separation.[18,21] Here, one phase is composed of almost equal proportions of PFB and F8BT whereas the second is F8BT-rich and consists of 80% F8BT and 20% PFB.

Further analysis revealed that the blend layers can be described by PFB-rich cylinders surrounded by a F8BT-rich matrix. Assuming the interface between those two phases to be cylindrical in shape with a height equal to the film thickness, a linear correlation was found between the interfacial area (per unit area of the layer) and the measured quantum efficiency. In fact, the 1:5 PFB:F8BT layer exhibited the largest interfacial area of 0.46 μm^2 per μm^2 film and the largest IPCE of ca. 4.5%. It was concluded that charges generated near this interface are efficiently transported through the corresponding PFB- or F8BT-rich phases. On the contrary, charges generated in the bulk are more susceptible for charge trapping due to the absence of a direct percolation path for charge transport. Higher efficiencies of up to 14% could only reached by modifying the substrate by microcontact printing with self-assembled monolayers and using isodurene as the solvent.[14] This has been attributed to a vertical phase separation.

In conclusion, these studies clearly showed that the preparation conditions as well as the layer composition have a profound and, in part, not predictable effect on the solar cell properties. Moreover, since the mesoscale phase separation has been shown to strongly depend on the blend ratio, an investigation for a given length scale of phase separation but different blend ratios was not possible by using layers spin-coated from organic solvents.

Recently, we proposed a novel approach to polymer blends based on polymer nanoparticles dispersed in water, which allows for a direct control of the length scale of the phase separation.[26−28] These nanoparticles are prepared using the miniemulsion method. In short, the polymers are first dissolved in a suitable solvent. Then, water containing a small amount of a suitable surfactant is added, and the whole mixture is sonicated for a short time until a homogeneous size distribution of the droplets of the resulting miniemulsion is reached. Evaporating of the organic solvent by gently heating the mixture gives a stable, aqueous dispersion of solid narrowly distributed polymer nanoparticles, with average particle diameters in the range from 30 to 300 nm.[29] Most important, this universal preparation method can be applied to a wide range of polymers as long they are soluble in a suitable (water-immiscible) organic solvent. Preliminary studies on nanoparticles containing a blend of PFB and F8BT revealed that the efficiency of photovoltaic devices based on these particles is not dependent on the solvent used in the miniemulsion process.[26] This indicated that it is not the kinetics of particle formation but rather the particle size and composition which controls the device efficiency.

Here, we use the particle approach to impose a fixed length scale of phase separation in PFB:F8BT layers. The optical properties of the blend layers composed either of single-component particles or of particles containing both polymers in each individual nanosphere are investigated for different ratios of PFB and P8BT. These data are used to interpret the dependence of the solar cell efficiency on the layer composition.

This paper is divided into two parts. In the first part we present absorption and photoluminescence measurements on dilute dispersions of nanospheres in water containing a blend of PFB and F8BT in each sphere. These nanospheres are prepared by the miniemulsion process starting from either the pure polymer or a mixture of PFB and F8BT. In the second part we present a detailed discussion of the properties of solar cells based on polymer nanoparticles. The two different approaches to form a nanostructured polymer blend are compared, either using a mixture of two single-component polymer particles or using the two-component blend particles (Figure 1b).

Experimental Section

Synthesis of the Aqueous Polymer Dispersions. Dispersions were prepared from PFB and F8BT polymers, purchased from American Dye Sources. Single polymer solutions in chloroform or solutions of the two polymers in chloroform (at 2.5 wt %) were added to an aqueous sodium dodecyl sulfate (SDS) (100 mg of SDS/10 g of water) solution. After stirring 1 h for preemulsification, the miniemulsion was prepared by sonicating the mixture for 2 min. The samples were left under stirring for 30 min at 62 °C to evaporate the chloroform from the liquid droplets in order to obtain an aqueous dispersion. To eliminate the excess of surfactant and concentrate the samples, they were ultrafiltered in centrifuge tubes (Amicon Ultra-4 centrifugal filter, 10 000 molecular weight cutoff). The final dispersions had 7% of solid content and 5% SDS to the amount of polymer. The particles sizes were measured using a Nicomp particle sizer at a fixed scattering angle of 90°.

Table 1. Compositions and Properties of the Polymer Nanoparticle Dispersions Containing Different Weight Ratios of PFB and F8BT

sample ID	weight ratio PFB:F8BT	mass of PFB (mg)	mass of F8BT (mg)	mean diameter (nm)
1_1D53	1:1	35	35	53
1_0D43	1:0	100		43
0_1D43	0:1		100	43
5_1D54	5:1	50	10	54
1_5D40	1:5	10	50	40
2_1D155	2:1	30	15	155
1_2D96	1:2	15	30	96
1_2D45	1:2	10	20	45
2_1D49	2:1	20	10	49

The particle compositions and particle diameters are summarized in Table 1.

Spectroscopy. Absorption spectra were recorded with a Perkin-Elmer LS 50 luminescence spectrometer. The spectra were corrected for the transmission of the uncoated glass slides in the case of film measurements and for the transmission of the cuvettes in the case of dispersions measurements.

Fluorescence spectra were measured with a Perkin-Elmer LS 50 luminescence spectrometer. The excitation was incident at an incident angle of 60° onto the front face of the sample, and the emission was recorded in reflection at an angle of 30°.

For time-resolved fluorescence measurements, the diluted dispersions were excited with a mode-locked Ti:sapphire laser (Tsunami, Spectra Physics) after second harmonic generation at $\lambda_{ex} = 392$ nm. The fluorescence of the samples was detected by a streak camera (C5680, Hamamatsu) equipped with an imaging spectrograph (250is, Chromex). The streak camera was operated in the sync mode at 80.2 MHz. The time-resolved measurements were performed using two time windows of 3495 and 1998 ps. The imaging spectrograph was set to a central wavelength of 590 nm, yielding a total spectral range of 413.5 nm $< \lambda_{em} <$ 819 nm. The time-resolved fluorescence spectra (TRES) were recorded in the single-photon counting mode. For each TRES 1000 images (608 ms integration time each) were accumulated. TRES were evaluated in slices of 10 nm, and the fluorescence decay times were determined using the lifetime fitting module TA-Fit (Hamamatsu).

Solar Cell Preparation and Characterization. In the first step, a thin layer of poly(ethylene dioxythiophene) doped with poly(styrenesulfonic acid) (PEDOT:PSS) (H.-C. Starck) was spin-coated at 2400 rpm onto glass substrates coated with indium−tin oxide (ITO) which were purchased from Merck. PEDOT:PSS is commonly used for organic electronic devices since it lowers the electrode work function of ITO (4.8 eV) to ca. 5.1 eV. In addition, it is known to reduce the surface roughness of the underlying ITO layer and thus the probability for electrical shorts.

The PEDOT:PSS films were dried by heating on a hot plate under a nitrogen atmosphere for 30 min at 170 °C. In the second step, the nanoparticles were spin-coated from the aqueous dispersions at 4200 rpm, which led to monolayers of particles as demonstrated in earlier work.[29] The layer thickness is then equivalent to the particle diameter. It was also shown that spin-coating a mixture of particles (fabricated from different polymers) with roughly the same particle size results in layers with a statistical distribution of the two kinds of particles.[26] The devices were completed by evaporating a 25 nm Ca layer protected by 100 nm Al at a base pressure of 2×10^{-6} mbar. The active solar cell area as defined by the geometrical overlap between the bottom ITO electrode and the top cathode was 0.25 cm^2.

All device characterization was performed under a nitrogen atmosphere. The quantum efficiency as a function of wavelength was measured with an Oriel 150 W Xe lamp in combination with an Oriel Cornerstone 260 monochromator.

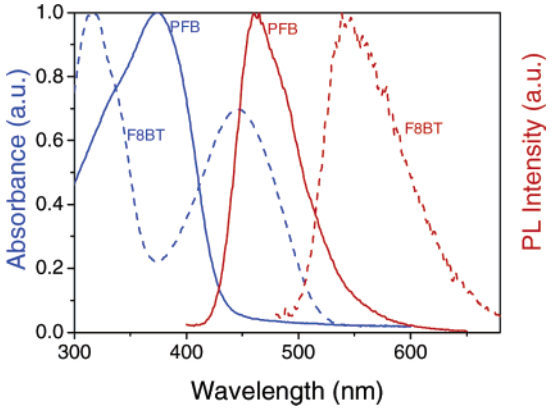

Figure 2. Absorption (blue) and photoluminescence spectra (red) of PFB (solid line) and F8BT (dashed line), recorded for an excitation wavelength of 380 nm.

The number of photons for each wavelength was calculated by using a calibrated Si diode as reference. The intensity of the monochromatic light was ca. 10 mW/cm^2. The incident-photon-to-converted-electron-efficiency (IPCE) was calculated by the number of electrons leaving the device divided by the number of incident photons. Current vs voltage $I(U)$ curves were recorded with a Keithley 2400 source/measure unit in the dark and under illumination with the full Xe lamp spectrum at a power density of 100 mW/cm^2. The white light power was measured with a Gentec pyroelectric power meter.

Atomic Force Microscopy (AFM). AFM micrographs were acquired in the semicontact mode with a NT-MDT Solver P47H microscope. High-resolution cantilevers with a typical curvature radius of 10 nm and a typical resonant frequency of 255 kHz were used.

Results and Discussion

1. Absorption and Photoluminescence Measurements on Diluted Dispersions. All dispersions and layers were characterized by optical absorption and photoluminescence spectroscopy. In particular, the degree of photoluminescence quenching was used as a measure of the degree of photoinduced charge transfer between PFB and F8BT. PFB and F8BT are well-suited for quenching experiments since their absorption and photoluminescence maxima are well-separated (Figure 2). PFB has its maximum emission at 460 nm, whereas the F8BT emission peaks at 540 nm.

The following sections present a detailed discussion of the photoluminescence properties in blend particles listed in Table 1. All measurements were performed on diluted aqueous dispersions (solid content about 5×10^{-4} wt %) to prevent reabsorption. For the photoluminescence measurements an excitation wavelength of 380 nm, which corresponds to the absorption maximum of PFB, and of 460 nm, which almost exclusively excites F8BT, were chosen.

First, the photoluminescence intensities of the single-component particle dispersions were measured and normalized to the absorption of the dispersions at the excitation wavelength. Then, the absorption spectra of the two-component blend particles were deconvoluted into the single-component spectra, from which the mass ratio of the two polymers in the blend particles was obtained. Based on these data, the expected photoluminescence spectra in absence of any quenching were calculated by adding the emission spectra of the pure particles in a ratio equivalent to the mass ratio as obtained above. Finally, the degree of quenching for each component was estimated as the ratio between measured photoluminescence and expected photoluminescence intensity.

As shown in Figure 3a, the PFB emission is severely quenched as soon F8BT is present in the particle. A fraction of 1:5F8BT:PFB per weight is sufficient to quench nearly all PFB emission. The F8BT emission as a function of PFB concentration shows a more gradual behavior. Even for particles with a 5/6 PFB solid content, the emission from F8BT is still 1/5 of its emission intensity in the absence of quenching.

To get more insight into the dynamics of the exciton recombination, time-resolved spectra of diluted nanoparticle dispersions were recorded. Using an excitation wavelength of 394 nm, both PFB and F8BT were excited. The PFB emission was averaged in a range of 440−480 nm and the F8BT emission in a range of 540−580 nm. The transients could be fitted with a mono-exponential decay function with a goodness of fit of $\chi^2 < 1.5$.

The decay time constant was found to be 500 ps for the pure PFB particles and 380 ps for the pure F8BT particles. As shown in Figure 3b, the PL decay of the PFB emission becomes much faster as soon as F8BT is present in the particle, consistent with the stationary PL emission experiments described before. For a ratio PFB:F8BT of 2:1, the observed PFB luminescence decay is on the order of the instrument response times. In this case, the upper limit for the decay time constant is given by the instrument response of 10 ps. In contrast, the time constant for the F8BT emission in PFB:F8BT 1:2 blend particles is only reduced to half of its value measured for pure particles. The time-resolved experiments indicate that the dissociation of a photogenerated exciton on a PFB chain occurs in less than 10 ps, whereas the dissociation of photogenerated excitons on F8BT is nearly 1 order of magnitude slower.

Transient absorption dynamic studies on F8BT have found a quite small value for the exciton diffusion constant of $D = 2.6 \times 10^{-4}$ cm^2 s^{-1}.[22] The exciton diffusion length l can then be calculated from the diffusion constant and the measured exciton decay time constant for F8BT by $l = \sqrt{\tau D}$, resulting in $l = 3.1$ nm. This value is well comparable to the value of $l = 5$ nm as extracted from the numerical modeling of bilayer devices.[16] Since the diffusion length is very small in F8BT, the particular particle morphology and the distribution of interfaces in the material are of special importance when discussing the dissociation of excitons formed on F8BT. Unfortunately, no data on the exciton diffusion length on PFB is presently available.

The data in Figure 3 show a pronounced asymmetry concerning the dependence of the degree of PL quenching on the particle composition. Apparently, a F8BT concentration of 20 wt % in PFB is sufficient to dissociate almost all excitons generated on the PFB phase. This experimental findings is in agreement with the previously published theory that the F8BT will easily penetrate PFB, leading to a very fine scale phase separation of F8BT in the PFB-rich phase, but not vice versa.[10,18]

With respect to the radiative decay of excitons on F8BT, blending F8BT with 20 to ca. 66 wt % PFB only gradually reduces the emission intensity, and the PL efficiency of F8BT remains within 50−70% of the pure particle value. Moreover, the F8BT decay time is almost constant for these blend ratios. This is indicative of a morphology as described above, with a phase containing

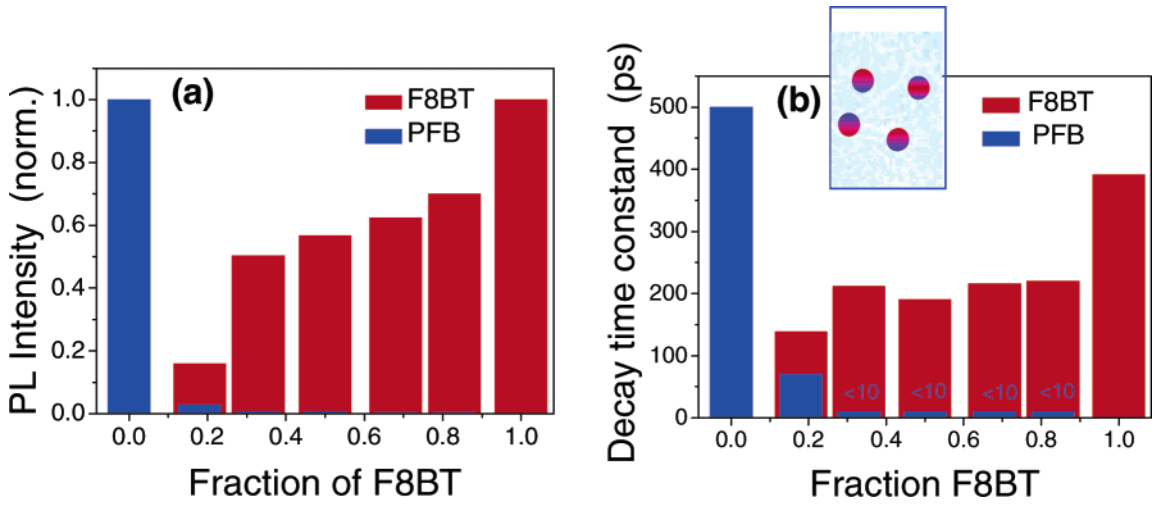

Figure 3. (a) Quenching of the photoluminescence of the PFB phase (blue), excited at 380 nm, and the F8BT phase (red), excited at 460 nm, for different ratios of PFB:F8BT in each particle. (b) Fluorescent decay times obtained from time-resolved photoluminescence spectra for the PFB emission (blue) and the F8BT emission (red) (excitation 394 nm) in pure and blend particles for different ratios.

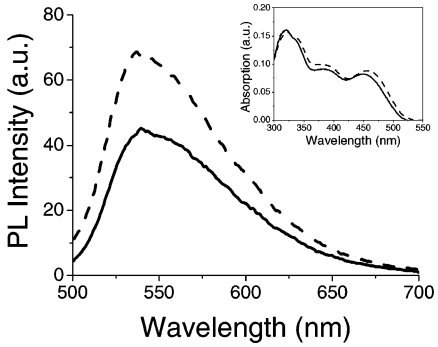

Figure 4. Absorption (inset) and photoluminescence spectra of emulsions containing PFB and F8BT in a ratio of 1:2 (excitation of the F8BT at 460 nm). The PFB emission upon excitation of 380 nm is completely quenched in both cases (not shown here). The particle diameter was 45 nm (solid) and 96 nm (dashed).

almost exclusively F8BT and a fine scale phase-separated phase of PFB and F8BT. In this picture, only a small fraction of excitons generated on the pure F8BT phase dissociate at the F8BT/PFB interface due to the small exciton diffusion radius. In contrast, almost all excitations in the blend phase decay nonradiatively. Reducing the F8BT concentration in the particle will then mostly decrease the size of the pure F8BT phase, while a considerably amount of F8BT is still contained in the PFB:F8BT mixed phase. In agreement with this interpretation, both the integrated F8BT emission intensity and the fluorescence lifetime drop considerably for a PFB:F8BT ratio of 5:1. Apparently, almost all F8BT molecules are now contained in the PFB:F8BT mixed phase.

To provide further information on the mesoscopic structure of the blend particles, particles containing PFB and F8BT in a ratio 1:2 were prepared with 45 and 96 nm mean diameter. Both dispersions have similar weight contents as proven by the nearly identical absorption spectra, as shown in the inset of Figure 4. If phase separation occurred on the length scale of the particle diameters, smaller particles should show a higher degree of quenching. As shown in Figure 4, the PL emission intensity of F8BT is considerably reduced for the 45 nm particles. Further experiments with other compositions and different particle diameters are in progress.

2. Nanoparticle Solar Cells. *Layers Prepared from Particle Blends.* Photovoltaic devices were prepared with varying ratios of PFB and F8BT in a range of 5:1 to 1:5. These devices were compared to the properties of diodes containing either pure PFB or pure F8BT particles.

Since the glass transition temperature of both polymers is well above room temperature, the particles retain their spherical shape after spin-coating. Therefore, the solid particles in the as-prepared layers have only few contact points In addition, as-prepared layers exhibit voids between the particles. Therefore, solar cells from as-prepared nanoparticle layers had low efficiencies and high leakage currents. To improve the contact between the particles and to fill the void in between, the layers were annealed at 150 °C for 2 h in a nitrogen atmosphere. As shown in the atomic force microscopy (AFM) picture in Figure 5, annealing leads to a flattening of the particles and the formation of a more homogeneous surface. Because of a tip curvature of 10 nm, the AFM cantilever can only penetrate a small distance between two particles, such that the actual particle topography is convoluted with the tip curvature.

The increase in interparticle contact area was documented by recording PL spectra after annealing at different temperatures, as shown in Figure 6. As-prepared layers consisting of PFB particles and F8BT particles in a ratio of 1:5 exhibit a strong PFB fluorescence upon excitation at 380 nm. The emission is only weakly quenched by adjunct F8BT particles due to the small interface. After annealing the layer at 150 °C, the situation changed dramatically. The PFB emission is fully quenched, whereas the F8BT emission is nearly unchanged. AFM measurements revealed that at this temperature the PFB particles have deformed, leading to a large interfacial area between PFB and F8BT. This results in an efficient quenching of the PFB fluorescence. On the other hand, the F8BT emission is almost not affected. This lack of quenching of the F8BT emission is still not fully understood, but we presume that the small exciton diffusion coefficient of F8BT imposes a strong limit on the fraction of excitons reaching the interparticle interface.

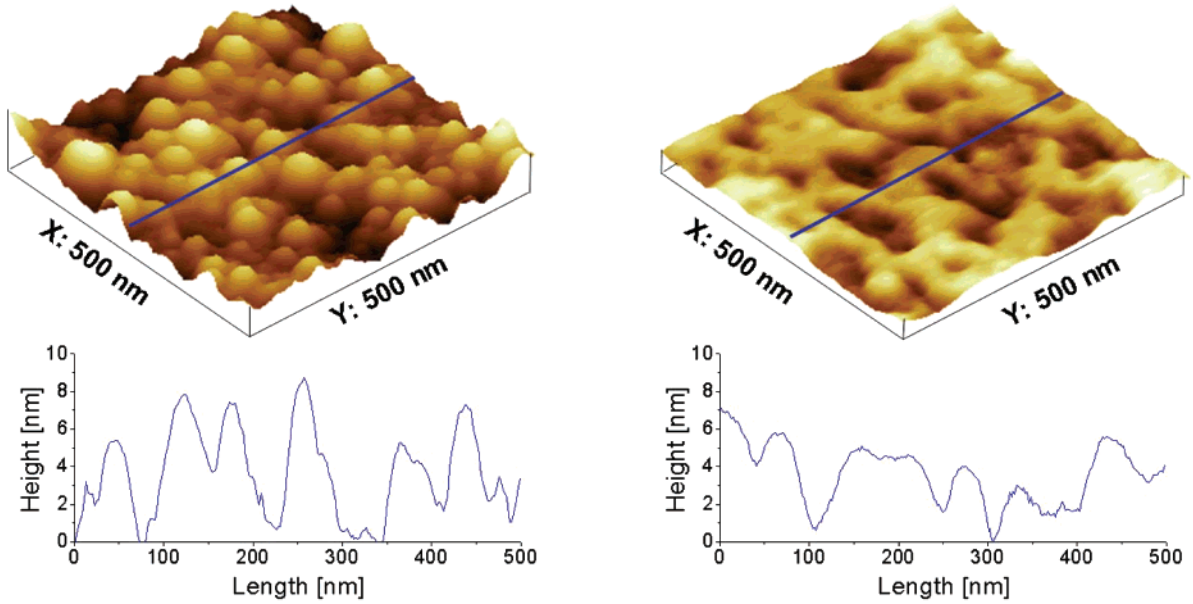

Figure 5. Atomic force microscope (AFM) height image and surface profile of a film prepared from dispersion 2_1D49 before (left) and after annealing (right) at 150 °C.

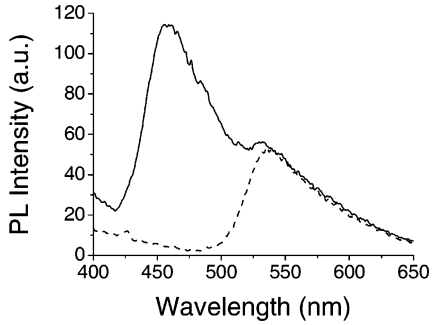

Figure 6. PL spectra of a layer consisting of PFB and F8BT particles in a ratio of 1:5, before (solid line) and after (dashed line) annealing of the device at 150 °C under a nitrogen atmosphere.

Figure 7 shows the incident photon to converted electron current efficiency (IPCE) as a function of wavelength of solar cells containing particle blend layers with different compositions. The spectra roughly resemble the spectral features of the both species. It is, therefore, meaningful to compare the quantum efficiencies at a wavelength of 380 nm (where mostly PFB absorbs) and 445 nm (at which F8BT absorbs almost exclusively) as a function of layer composition.

As shown in Figure 8a, the highest efficiency (ca. 2%) was measured for the mixture of particles with the highest concentration of PFB in the layer. Note that devices containing only PFB particles showed a much lower efficiency, well below 0.4%. The IPCE efficiency of blend devices with excitation at 380 nm decreases nearly linearly with increasing F8BT content in the layer. This indicates that the photocurrent at 380 nm is almost completely determined by the fraction of light absorbed by the PFB phase. This result is quite surprising as it suggests that the fraction of excitons generated in the PFB particles which dissociates into free charges is constant and independent of the F8BT fraction. Apparently, all excitons generated within a certain volume of the particles are able to diffuse either to the interparticle interface (and dissociate via electron transfer to the F8BT phase) or to the cathode (which then

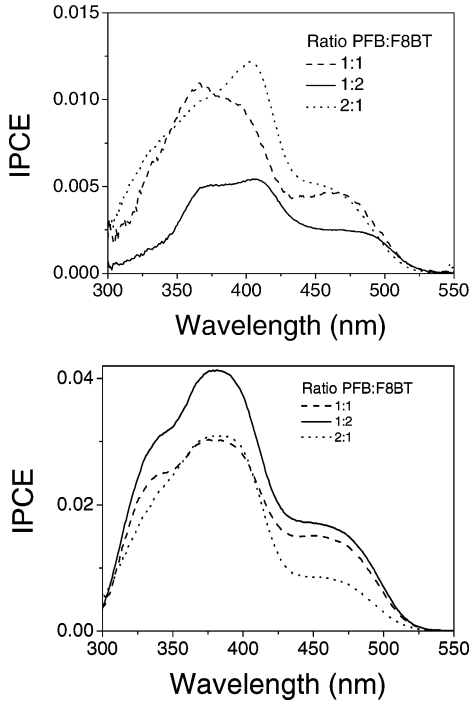

Figure 7. IPCE spectra of PFB:F8BT devices prepared from a blend of different particles (top) and for devices containing multicomponent blend particles (bottom).

acts as an electron acceptor), independent of the layer composition. The interpretation that electron transfer to the cathode contributes to the dissociation of PFB excitons is supported by the shape of the IPCE spectra: the peaks in the IPCE spectra of the PFB:F8BT blends are either red- or blue-shifted with respect to the PFB absorption maximum. This indicates the presence of inner-filter effects: At the wavelength of maximum absorption, the penetration depth of light is smallest, and most excitons are formed close to the electrode through which light enters the layer (which is opposite to the electron-harvesting cathode). For longer (or shorter) wavelengths, the penetration depth increases, and a larger fraction of excitons are generated close to

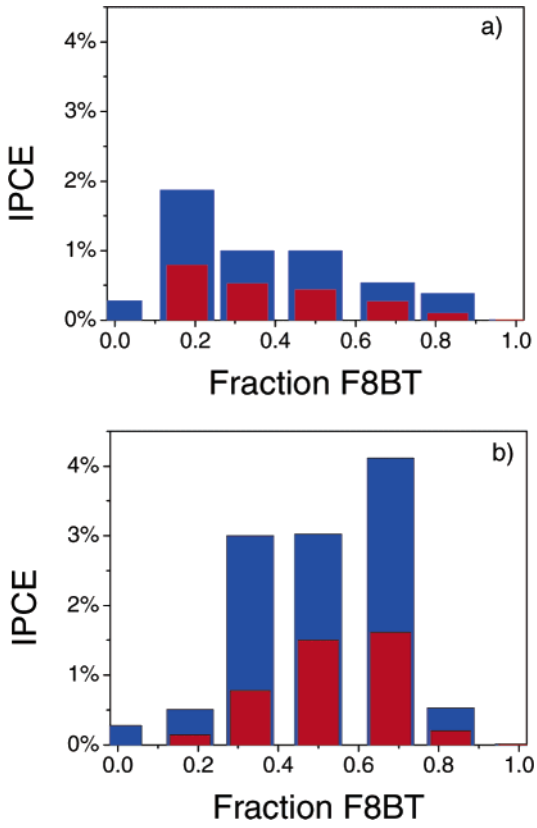

Figure 8. IPCE at 380 nm (blue) and at 445 nm (red) for (a) devices with a blend of different particles and (b) for devices containing a polymer blend in each particle.

the cathode. Note that in contrast to the studies on conventional blend layers (spin-coated from organic solvents) the length scale of phase separation in the nanoparticle layer is constant and independent of the composition. As a consequence, the probability that excitons formed on the PFB phase reach the interparticle interface is the same for all compositions. Therefore, the IPCE is expected to be solely determined by the statistical probability that excitons at the particle interfaces dissociate into free carriers and by the probability that these carriers are collected by the electrodes.

Opposed to our expectation, a higher F8BT content did not lead to a higher efficiency at 445 nm. Apparently, the larger total number of excitons generated on the F8BT phase for increasing F8BT particle concentration is accompanied by a strongly decreasing dissociation probability. This effect can be explained by simple geometric considerations. For the sake of simplicity we assume hexagonal packing, where each particle has six nearest neighbors. It should be noted that true hexagonal packing can only be reached for monodisperse particles (size variation <2%) on a completely flat surface. This is not the case for these experiments since there is a small size variation as seen in the AFM pictures and the ITO substrates with PEDOT/PSS are quite rough. Nevertheless, a nonideal packing should have only little influence on the following argumentation.

Following this consideration, in the PFB:F8BT 5:1 layer the F8BT particles are on average surrounded by five PFB and only one F8BT particle. On the other hand, for the 1:5 ratio, nearly all F8BT neighbors are also F8BT particles, and the dissociation of F8BT excitons by hole transfer to PFB is quite unlikely. We, therefore, propose that the photocurrent efficiency at 445 nm for different compositions is largely determined by the average number of PFB particles in direct contact with an F8BT particle.

Layers Prepared from Blend Particles. Solar cells prepared from dispersions containing a blend of PFB and F8BT in each particle behaved rather different compared to solar cells prepared from particle blends. First, as shown in Figure 8b, significantly higher solar cell efficiencies are measured. Moreover, the highest efficiency is now found for F8BT-rich blends. Note that a peak quantum efficiency of 4.2% measured for this device is among the highest values reported so far for PFB:F8BT blends, indicating efficient dissociation of excitons and transport of charges to the electrodes. Also, the maxima in the IPCE spectra (Figure 7 (bottom)) coincide exactly with the corresponding absorption maxima of the two polymers. This indicates that inner-filter effects play a minor role and that exciton dissociation at the interface to the cathode is insignificant.

The dependence of the IPCE efficiency as a function of the composition can be understood from the proposed morphology of the particles, taking into account the geometric constraints, as shown in Figure 9. To achieve high IPCE efficiencies, the electron-accepting phase must be in direct contact to the electron-withdrawing cathode (and the hole-accepting phase in contact to the PEDOT:PSS anode). In the case of the single-component particle blend layer discussed above, this condition is automatically fulfilled for all compositions. In contrast, for layers prepared from dual-component blend particles, the probability to extract both kinds of charges from the layer depends on the orientation and composition of the particles. Apparently, the optimum composition is determined by the condition that both phases take up approximately equal volumes in the particles. Since a pure F8BT phase is only formed above a certain concentration in the particles, we presume that the PFB:F8BT 1:2 blend (rather than the 1:1 blend) is closest to this optimum situation. As further expected, the IPCE efficiency is low for the 5:1 and 1:5 blend particles. In this case, only a small percentage of the nanospheres fulfills the conditions for efficient extraction of both kinds of charges.

As mentioned in the Introduction, it was proposed that the efficiency of the conventional PFB:F8BT blend devices increases linearly with the mesoscale interfacial area.[20] According to these results, an IPCE efficiency of 4.2% as measured here for the best device should correspond to an interfacial area of 0.42 μm^2 per μm^2 film area. Up to now, we do not have detailed information on the exact phase-separated structure in the blend particles. In a first step, we have estimated the interfacial area for particle layers by assuming that the blend particles consist of two-half spheres. The interfacial normalized to the layer area will then be $\pi(d/2)^2/\sqrt{(3/4)d^2} = 0.9$ for a hexagonal packing of the particles. This value is roughly a factor of 2 higher than the interfacial area of 0.42 μm^2 per μm^2 as estimated above. However, the samples studied by Snaith et al. exhibited a lateral phase separation, which is the ideal case with respect to charge extraction. For the blend in individual particles, the orientation of the interface to the substrate will be random as pictured in the scheme in Figure 9. Thus, the active interfacial area is expected to be half of the value estimated above (0.45 μm^2 per μm^2 of film).

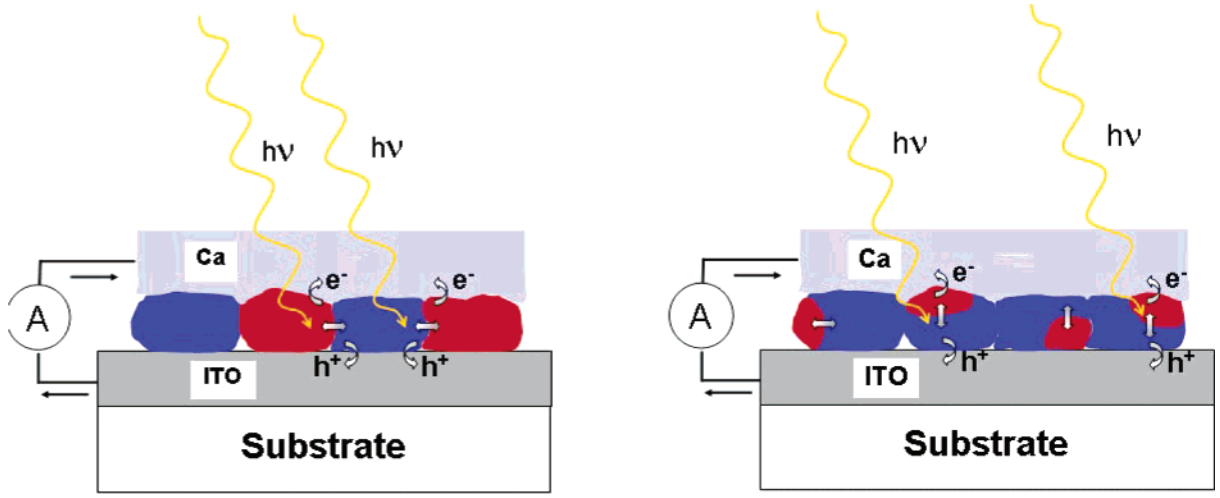

Figure 9. Schemes of solar cell devices based on a blend of different particles (left) and a blend of polymers in each particle (right scheme).

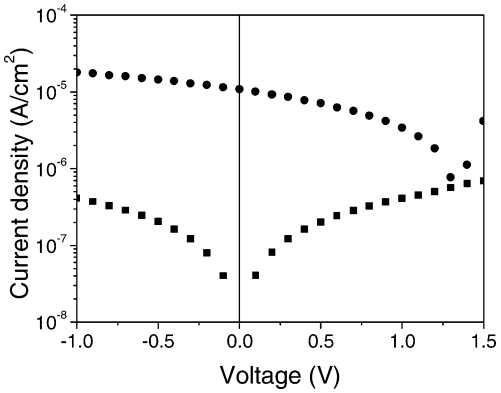

Figure 10. *I*(*U*) characteristics for a particle blend device containing 43 nm PFB particles and F8BT particles (blend ratio 1:2) in the dark (squares) and under white light illumination (circles) with an intensity of 100 mW/cm^2.

Current−Voltage Characteristics. Figure 10 shows typical current−voltage characteristics of a particle solar cell device in the dark and under illumination. The fill factor for these devices is in the range of 25%−28%, and the open-circuit voltage was as high at 1.38 V. All diodes prepared by the two different approaches for different compositions exhibited rather similar characteristics, without any obvious differences in the shape of the *I*(*U*) curves. The large open-circuit voltage and the low dark current indicate that excellent layers without any void can be formed with spin-coating the nanospheres. Further, the fill factor is in the range of the values reported previously for conventional polymer−polymer blends, and there is no indication for any additional barriers between the particles and the electrodes. Note that much higher fill factors >40% were only obtained for devices incorporating strong electron acceptors such as PCBM,[3] TiO_2,[30] or CdSe,[31] possessing high electron mobilities.

We therefore presume that the only moderate electron mobility on most electron-accepting polymers is a major factor limiting the fill factor and thus the power conversion efficiency of polymer-based solar cells.

Conclusion

The possibility to control the dimension of phase separation in polymer blend layers by using polymer nanoparticles opens new ways to study the influence of the layer composition on the solar cell performance. In layers composed of mixtures of single-component particles of PFB and F8BT, a laterally phase-separated structure in imposed, in which the solar cell efficiency should be mainly determined by the probability that excitons formed on the two phases dissociate into free carriers. Further, since the particle size is nearly constant, the fraction of excitons reaching the interparticle interface is expected to be independent of the layer composition. Therefore, the dependence of the efficiency of these particle blend layers on the layer composition should be mainly determined by the probability of the excitons to dissociate at the particle interface. Surprisingly, the external quantum efficiency is highly asymmetric with respect to the PFB:F8BT ratio. In fact, the IPCE measured under illumination conditions which excites excitons primarily on either the PFB or the F8BT particles decreases almost linearly with decreasing PFB concentration. We further presume that this particular effect is due to a rather small exciton diffusion length on the F8BT phase. As a consequence, the fraction of excitons on a F8BT particle that dissociate into free carriers is linearly proportional to the interfacial area formed by direct contact with adjacent F8BT and PFB particles.

In contrast, the IPCE of layers prepared from blend particles containing both polymers in each nanosphere is rather symmetric with respect to the composition. We presume that the IPCE of these devices is strongly determined by the probability that both kinds of charge carriers generated by the dissociation of excitons on a blend particle can be extracted to the corresponding electrodes. This probability should depend on both the orientation and composition of the particles. Apparently, the optimum composition is determined by the condition that both phases take up approximately equal volumes in the particles. In our layers, the highest quantum efficiency of about 4% is measured for nanoparticles with a weight ratio PFB:F8BT of 1:2. This indicates that a slightly larger amount of F8BT is necessary in the blend particles to obtain optimum conditions for exciton dissociation and charge extraction. On the basis of our photoluminescence results and studies on the morphology of conventional PFB:F8BT blends as published by others, we presume that a certain fraction of the F8BT polymers are embedded into the PFB phase and that a separate F8BT phase is only formed above a certain

concentration in the particles.

Finally, we note that an external quantum efficiency of 4% measured for devices containing 1:2 PFB:F8BT particles is among the highest values reported so far for this material combination. On the other hand, this value is rather small, considering the almost complete quenching of the PFB emission in the blend particles. On the basis of our spectroscopic studies, we propose that both the tendency of F8BT to penetrate the PFB phase and a small exciton diffusion length on F8BT are the most crucial factors limiting the efficiency of these devices. Therefore, our future work will primarily focus on particles prepared from highly immiscible polymers, allowing for a better control of the particle blend morphology and thus of the structure of the resulting polymer blend layers.

Acknowledgment. We thank Prof. Dr. H.-G. Löhmannsröben and Dr. W. Regenstein (University of Potsdam) for the access to their optical spectrometers used in this work. We also acknowledge the financial support by the Stiftung Volkswagenwerk, the Fond der chemischen Industrie, and the Max-Planck-Society.

References and Notes

(1) Yu, G.; Gao, J.; Hummelen, J. C.; Wudl, F.; Heeger, A. J. *Science* **1995**, *270*, 1789−1791.
(2) Halls, J. J. M.; Walsh, C. A.; Greenham, N. C.; Marseglia, E. A.; Friend, R. H.; Moratti, S. C.; Holmes, A. B. *Nature (London)* **1995**, *376*, 498−500.
(3) Brabec, C. J.; Sariciftci, N. S.; Hummelen, J. C. *Adv. Funct. Mater.* **2001**, *11*, 15−26.
(4) Krausch, G. *Mater. Sci. Eng. R* **1995**, *14*, 1−94.
(5) Jones, R. A. L.; Norton, L. J.; Kramer, E.; Bates, F. S.; Wiltzius, P. *Phys. Rev. Lett.* **1991**, *66*, 1326−1329.
(6) Shaheen, S. E.; Brabec, C. J.; Sariciftci, N. S.; Padinger, F.; Fromherz, T.; Hummelen, J. C. *Appl. Phys. Lett.* **2001**, *78*, 841−843.
(7) Walheim, S.; Böltau, M.; Mlynek, J.; Krausch, G.; Steiner, U. *Macromolecules* **1997**, *30*, 4995−5003.
(8) Böltau, M.; Walheim, S.; Mlynek, J.; Krausch, G.; Steiner, U. *Nature (London)* **1998**, *391*, 877−879.
(9) Müller-Buschbaum, P.; Gutmann, J. S.; Stamm, M. *Macromolecules* **2000**, *33*, 4886−4895.
(10) Halls, J. J. M.; Arias, A. C.; MacKenzie, J. D.; Wu, W. S.; Inbasekaran, M.; Woo, E. P.; Friend, R. H. *Adv. Mater.* **2000**, *12*, 498−502.
(11) Johansson, D. M.; Theander, M.; Granlund, T.; Inganäs, O.; Anderson, M. R. *Macromolecules* **2001**, *34*, 1981−1986.
(12) Schmitt, C.; Nothofer, H.-G.; Falcou, A.; Scherf, U. *Macromol. Rapid Commun.* **2001**, *22*, 624−628.
(13) Sun, S. *Sol. Energy Mater. Sol. Cells* **2003**, *79*, 257−264.
(14) Arias, A. C.; Corcoran, N.; Banach, M.; Friend, R. H.; MacKenzie, J. D. *Appl. Phys. Lett.* **2002**, *80*, 1695−1697.
(15) Arias, A. C.; MacKenzie, J. D.; Stevenson, R.; Halls, J. J. M.; Inbasekaran, M.; Woo, E. P.; Richards, D.; Friend, R. H. *Macromolecules* **2001**, *34*, 6005−6013.
(16) Barker, J. A.; Ramsdale, C. M.; Greenham, N. C. *Phys. Rev. B* **2003**, *67*, 075205/1-9.
(17) Morteani, A. C.; Dhoot, A. S.; Kim, J.-S.; Silva, C.; Greenham, N. C.; Murphy, C.; Moons, E.; Cina, S.; Burroughes, H.; Friend, R. H. *Adv. Mater.* **2003**, *15*, 1708−1712.
(18) Ramsdale, C. M.; Bache, I. C.; MacKenzie, J. D.; Thomas, D. A.; Arias, A. C.; Donald, A. M.; Friend, R. H.; Greenham, N. C. *Physica E* **2002**, *14*, 268−271.
(19) Ramsdale, C. M.; Barker, J. A.; Arias, A. C.; MacKenzie, J. D.; Friend, R. H.; Greenham, N. C. *J. Appl. Phys.* **2002**, *92*, 4266−4270.
(20) Snaith, H. J.; Arias, A. C.; Morteani, A. C.; Silva, C.; Friend, R. H. *Nano Lett.* **2002**, *2*, 1353−1357.
(21) Stevenson, R.; Arias, A. C.; Ramsdale, C. M.; MacKenzie, J. D.; Richards, D. *Appl. Phys. Lett.* **2001**, *79*, 2178−2181.
(22) Stevens, M. A.; Silva, C.; Russel, D. M.; Friend, R. H. *Phys. Rev. B* **2001**, *63*, 165213−116521.
(23) Redecker, M.; Bradley, D. D. C.; Inbasekaran, M.; Wu, W. W.; Woo, E. P. *Adv. Mater.* **1999**, *11*, 241−246.
(24) Campbell, A. J.; Bradley, D. D. C.; Antoniadis, H. *Appl. Phys. Lett.* **2001**, *79*, 2133−2135.
(25) Fung, M. K.; Tong, S. W.; Lai, S. L.; Bao, S. N.; Lee, C. S.; Wu, W. W.; Inbasekaran, M.; J. J.; O. B.; Liu, S. Y.; Lee, S. T. *J. Appl. Phys.* **2003**, *94*, 2686−2694.
(26) Kietzke, T.; Neher, D.; Landfester, K.; Montenegro, M.; Güntner, R.; Scherf, U. *Nat. Mater.* **2003**, *2*, 408−412.
(27) Kietzke, T.; Neher, D.; Montenegro, R.; Landfester, K.; Scherf, U.; Hörhold, H. H. *Proc. SPIE Int. Soc. Opt. Eng.* **2004**, *5215*, 206−210.
(28) Piok, T.; Gamerith, S.; Gadermaier, C.; Wenzl, F. P.; Patil, S.; Montenegro, R.; Kietzke, T.; Scherf, U.; Landfester, K.; Neher, D.; List, E. J. W. *Adv. Mater.* **2003**, *15*, 800−804.
(29) Landfester, K.; Montenegro, R.; Scherf, U.; Güntner, R.; Asawapirom, U.; Patil, S.; Neher, D.; Kietzke, T. *Adv. Mater.* **2002**, *14*, 651−655.
(30) Breeze, A. J.; Schlesinger, Z.; Carter, S. A.; Brock, P. J. *Phys. Rev. B* **2001**, *64*, 125205/1-9.
(31) Huynh, W. U.; Dittmer, J. J.; Alivisatos, A. P. *Science* **2002**, *295*, 2425−2427.

MA049625Y